CB-Note 342

# LEAR Crystal Barrel Experiment, PS197
# Normalization of the Finescan Data

Willi Roethel
Univ. Munich

December 8, 1998

# Contents

# 1 Introduction

This report is meant to describe the way the finescan data was normalized. The first part deals in general with the scalers and everything around that and is meant for people who intend to work with these scalers. In this part the contents of the scaler bank is listed together with some read out methods and aspects of the DAQ are discussed.

The second part of this report covers the application of the scalers to the data, i.e. the normalization. The cross sections for the reaction $\bar{p}p \to \pi^0\pi^0$ are given and the results of cross checks, done as well with other channels as with different triggers are shown to prove the reliability of the cross section values. Finally a beam rate dependence of the cross sections of the finescan data is examined.

A reader not interested in the technical recipe of the normalization may skip the first part right away start with section 3.

# 2 Scalers

## 2.1 The Scaler Bank RSCL

The Scaler Bank 'RSCL' contains the information of the beam counters including KC and the Silicon Counters as well as the output of various programmable logical units (PLUs). An old version of the RSCL bank is already described in the CB offline manual (CB-Note 121) citecboff. Since then two new scalers have been introduced to measure the lifetime of the detector. The bank is addressed using the link LRSCL (in the common block CBLINK) and consists of 29 data words. The contents of the bank in it latest form is described in table 1.

For the read out of the scaler bank it is necessary to know that every entry in the scaler bank is a 32 bit word made up from two 16 bit words. The order of the most significant byte (MSByte) and least significant byte (LSbyte) changes twice in the bank. Table 1 gives the order of the MSByte and LSByte for every value in the scaler bank. In Appendix B the Fortran function SCL_FSWAP, written by Klaus Peters and originally used in the online trigger monitor program is listed to provide a simple way to extract the information of those scalers with bits $1 \ldots 16$ holding the most significant byte and bits $17 \ldots 32$ the least significant byte. The value for the lower left Silicon counter would then be read out using

SI_LD = SCL_FSWAP(IQ(LRSCL+3))

| Offset | Type | byte ordering | Content |
|---|---|---|---|
| +1 | Integer | | word counter |
| +2 | Integer | msb(1..16) lsb(17..32) | Silicon Right Down |
| +3 | Integer | msb(1..16) lsb(17..32) | Silicon Left Down |
| +4 | Integer | msb(1..16) lsb(17..32) | Silicon Right Up |
| +5 | Integer | msb(1..16) lsb(17..32) | Silicon Left Up |
| +6 | Integer | msb(1..16) lsb(17..32) | Silicon Center |
| +7 | Integer | msb(1..16) lsb(17..32) | Silicon High |
| +8 | Integer | msb(1..16) lsb(17..32) | Kens Chamber (KC) |
| +9 | Integer | msb(1..16) lsb(17..32) | 10 kHz clock (test pulser) |
| +10 | Integer | | light 1(bits 1..16), americium 1 (bits 17..32) |
| +11 | Integer | | light 2(bits 1..16), americium 2 (bits 17..32) |
| +12 | Integer | lsb(1..16) msb(17..32) | PLU 1/ output 6 - $Si_C$.KC |
| +13 | Integer | lsb(1..16) msb(17..32) | PLU 2/ output 5 |
| +14 | Integer | lsb(1..16) msb(17..32) | PLU 2/ output 6 |
| +15 | Integer | lsb(1..16) msb(17..32) | PLU 3/ output 5 - KC.$\overline{\text{Veto}}$ |
| +16 | Integer | lsb(1..16) msb(17..32) | PLU 3/ output 6 - $Si_C$.KC.$\overline{Si_{High}}$ |
| +17 | Integer | lsb(1..16) msb(17..32) | PLU 4/ output 4 |
| +18 | Integer | lsb(1..16) msb(17..32) | PLU 4/ output 5 |
| +19 | Integer | lsb(1..16) msb(17..32) | PLU 5/ output 6 - $Si_C$.KC.$\overline{\text{Veto}}$ |
| +20 | Integer | lsb(1..16) msb(17..32) | PLU 5/ output 7 - pile-up |
| +21 | Integer | lsb(1..16) msb(17..32) | PLU 6/ output 6 - Backplane Veto 0-Prong |
| +22 | Integer | lsb(1..16) msb(17..32) | PLU 8/ output 6 - JDC Veto 0-Prong |
| +23 | Integer | lsb(1..16) msb(17..32) | PLU 7/ output 6 - System Reset |
| +24 | Integer | lsb(1..16) msb(17..32) | PLU 7/ output 7 |
| +25 | Integer | lsb(1..16) msb(17..32) | events accepted |
| +26 | Integer | lsb(1..16) msb(17..32) | fast resets |
| +27 | Integer | lsb(1..16) msb(17..32) | system resets |
| +28 | Integer | msb(1..16) lsb(17..32) | Life Time 16 MHz clock |
| +29 | Integer | msb(1..16) lsb(17..32) | Life Time 1 MHz clock |

Table 1: The Scaler Bank RSCL (The table was copied from Hartmut Kalinowskys file on the scaler bank. The original note can be found in the appendix A of this note)

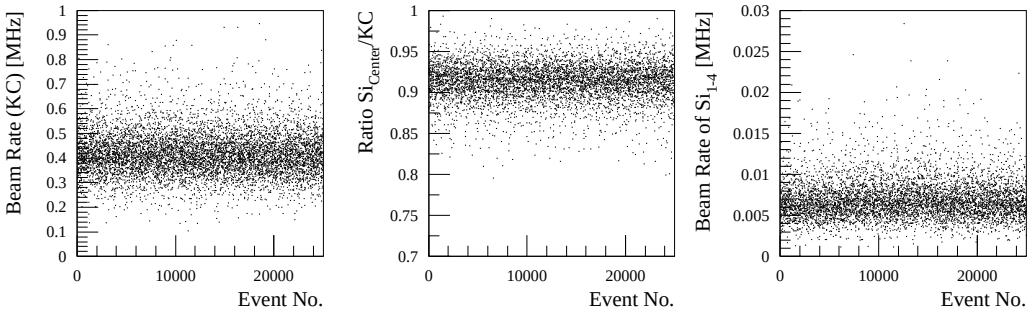


Figure 1: (from left to right) Beam Rate (Kens Chamber), Ratio of $Si_C$/KC, and $Si_{1-4}$ rate vs the event no. on tape (data for the finescan point at 1412 MeV/c).

Basically all scalers are the running sums of the values they hold, i.e. counts on the scaler values are always added to the previous values. In principle this allows to extract e.g. the number of incoming antiprotons using only a subsample of the original data sample. 'Basically' means all but the counts from the 16 MHz and 1 MHz clocks. The values of these scalers are always measured between two events. So in practice to extract the lifetime of the detector it is essential to look at all events. This can be quite annoying especially if it has to be done for large data samples.

A special remark has to be made on the output 6 of PLU 3 (word 16). Since the incoming beam is defined by $Si_C$.KC.$\overline{Si_{High}}$ this scaler should give the number of antiprotons to normalize to. Unfortunately this scaler was not working, at least for all the runs this report is based on. What has to be used instead is the output 6 of PLU 1 which gives $Si_C$.KC. The fraction of the $Si_{High}$ counts to $Si_C$ is about 0.4% and can be used to correct the value above but was considered negligible in this work.

The scalers now can be used, e.g. to reproduce the beam conditions while data taking. Figure 1 shows the beam rate as measured by Kens Chamber, the ratio $Si_C$/KC, which was a matter of interest in the October 96 run period, and the rate of the 4 outer segments of the five-fold Silicon counter, which gives an indication of the quality of beam alignment, all as a function of event on tape.

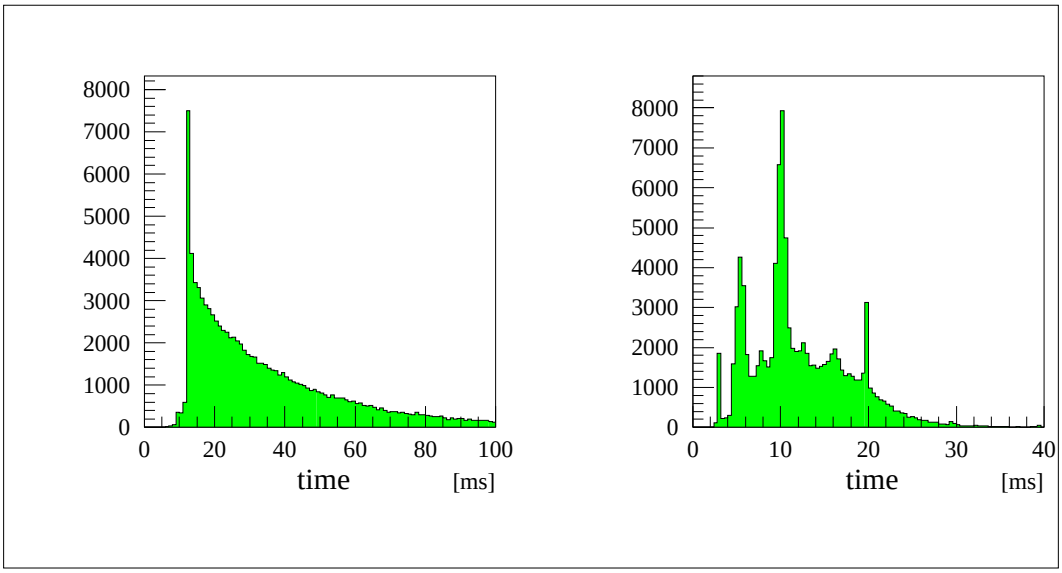


Figure 2: Time between two accepted events; left for the 0-Prong trigger, right for minimum bias

## 2.2 The Trigger System

A crucial part of the normalization is in the accurate monitoring of the lifetime of the detector. For this reason, in addition to the 10 kHz pulser recording the total time, two additional clocks were added to the system running at 16 MHz and 1 MHz respectively and monitoring the lifetime of the detector. The clocks start at the opening of the trigger gate and stop when the trigger gate closes with a delay of 4$\mu$s to allow for the drifting time in the JDC [2]. It seems necessary therefore to understand the trigger system in terms of lifetime and dead time and try to verify the correct measurement of the lifetime.

Looking at the time spectrum of the events (total dead time = total time - lifetime) as shown in the left plot of figure 2 for the 0-prong trigger it is easy to see that a minimum time of $\approx$12 ms is required for each event. This is the time needed to process an event accepted by the trigger system. It may be added that the same spectrum for minimum bias data shown in the right plot of figure 2 shows several peaks, the most prominent of these at 12 ms referring to the 'physical events'. Next to that another peak rises around 5 ms probably origining from empty events.

Taking this 12 ms dead time for the data processing of an accepted event, it can be tried to estimate the dependence of the lifetime ratio L = $t_{16\,\mathrm{MHz}}/t_{10\,\mathrm{kHz}}$ on the beam rate with some assumptions on the 'cross section' of the channel triggered on as seen by the detector. Neglecting the dead time

correction of the fast resets the lifetime ratio can be estimated as

$$L = \frac{t_{event}}{t_{event} + t_{proc}}$$

where $t_{proc} = 10$ ms is the time needed to process the data (minimum dead time) and

$$\begin{aligned} t_{event} &= 1/\text{reaction rate} \\ &= \frac{5.33 \cdot 10^3 \text{mb}}{\sigma \cdot R_{\bar{p}}} \end{aligned}$$

the avg. time between two accepted events with $\sigma$ being the cross section of the channel (as seen by the detector), $R_{\bar{p}}$ the beam rate and $5.33 \cdot 10^3$ mb the reaction rate in the target described in section 3 of this report.

Obviously this formula is only valid if the time between good events is large compared to dead times. For cases where the time between good events is close to the total time of the fast resets discussed in detail below the fast resets can not be neglected anymore but have to be added to the average time required for every event. Figure 3 shows the beam rate dependence of 0-prong data, 2-prong data and minimum bias data. The cross sections used to calculate these estimates were 1 mb for 0-prong, 30 mb for 2 prong and 100 mb for minimum bias. These values can only be estimates since we do not know what the 'effective cross sections' for the detector really are.

The simple the formula and the estimates it is based on are, the qualitative agreement with the measurement is quite remarkable. Cross checks on specific channels between minimum bias and 0-prong resp. 2-prong data give further support that the lifetime of the detector is measured correctly as will be shown in part 2 of this report.

## Fast Resets

If an event is accepted in trigger levels 0 (incoming beam and no Veto signal) and 1, the backplane signal of the Silicon Vertex Detector, it can still be rejected at higher levels using the JDC hit pattern and the energy deposit in the crystals from the Total Energy Trigger ('Tonys box'). As already mentioned before, the clocks for the lifetime measurement are stopped as soon as trigger level 2 is reached with a delay of $4\mu$s. If the event is rejected in the following the system is cleared with a so called fast reset. For the evaluation of the lifetime this $4\mu$s delay then has to be taken into consideration in that it has to be subtracted from the measured value of the lifetime ratio:

$$L = \frac{t_{16\,\text{MHz}} - N_{\text{fast resets}} \cdot 4\mu\text{s}}{t_{10\,\text{kHz}}}$$

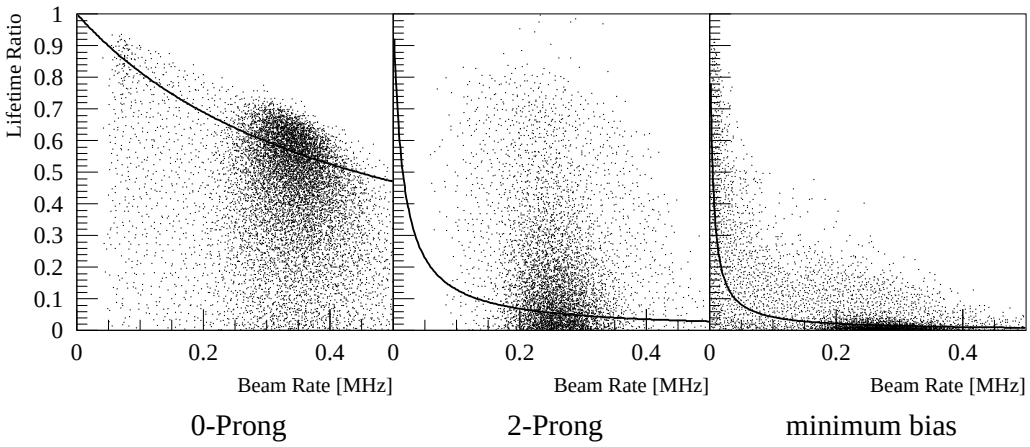


Figure 3: Lifetime Ratio (Lifetime of the trigger divided by the total time between two accepted events) as a function of the beam rate for (from left to right) 0-prong trigger at 1412 MeV/c, 2-Prong trigger at 1525 MeV/c and minimum bias also at 1525 MeV/c. Solid lines are expected dependence as described in the text.

An interesting (but somehow academic) feature is the evaluation of the dead time for every fast reset. Figure 4 shows the no. of fast resets as a function of the dead time of the system. Using the slope of the straight line one can estimate a time of $\approx 40\mu$s needed to reset the system.

## Beam Conditions at the Begin of Spills

The behavior of the beam at the beginning of spills has been a matter of some interest. The upper left plot of Fig. 5 shows the beam rate as seen by KC over the first 5000 events (refers to about 5 min.) of a spill and the dependence is not surprising. There is probably a small spike at the very beginning of a spill but this was usually cut off since the shutter was down at the beginning of spills (the reason being exactly that spike). After that the beam rate increases to the programmed value. What is surprising at first sight is the ratio of $\mathrm{Si_C}$/KC for the first events as shown in the upper right plot of figure 5. It seems that the $\mathrm{Si_C}$ counter has a small geometrical acceptance at the beginning of the spill and then rises to its usual value. This effect is not caused by a displaced beam since the only outer Silicon counter which is affected by this also shows the same inefficiency (lower plots of figure 5). A plausible explanation of this behavior would be that the beam at the beginning of the spills is defocused and only slowly gets into focus. Since KC has a larger opening angle the count rate will not to be

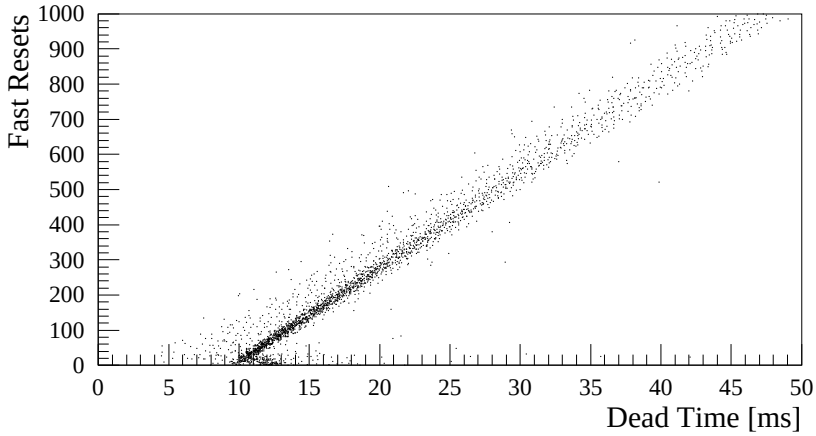


Figure 4: no. of fast resets between two accepted events vs. the dead time. The slope of the distribution gives the dead time per fast reset

effected so much by defocusing. However this behavior of the beam does not lead to any peculiar behavior of the lifetime measurement as the left plot in fig. 3 proves. The enhancement of points at the beam rates of about .16 MHz and a lifetime ratio of .9 corresponds to exactly these events shown in figure 5 but lies just around the area where one would expect the points to be.

It should be pointed out however that a ratio of 90% is not common throughout the scan. At some energies this ratio even goes down to values below 60%.

Summarizing all points mentioned in this section - one can say that the triggers show no peculiar behavior.

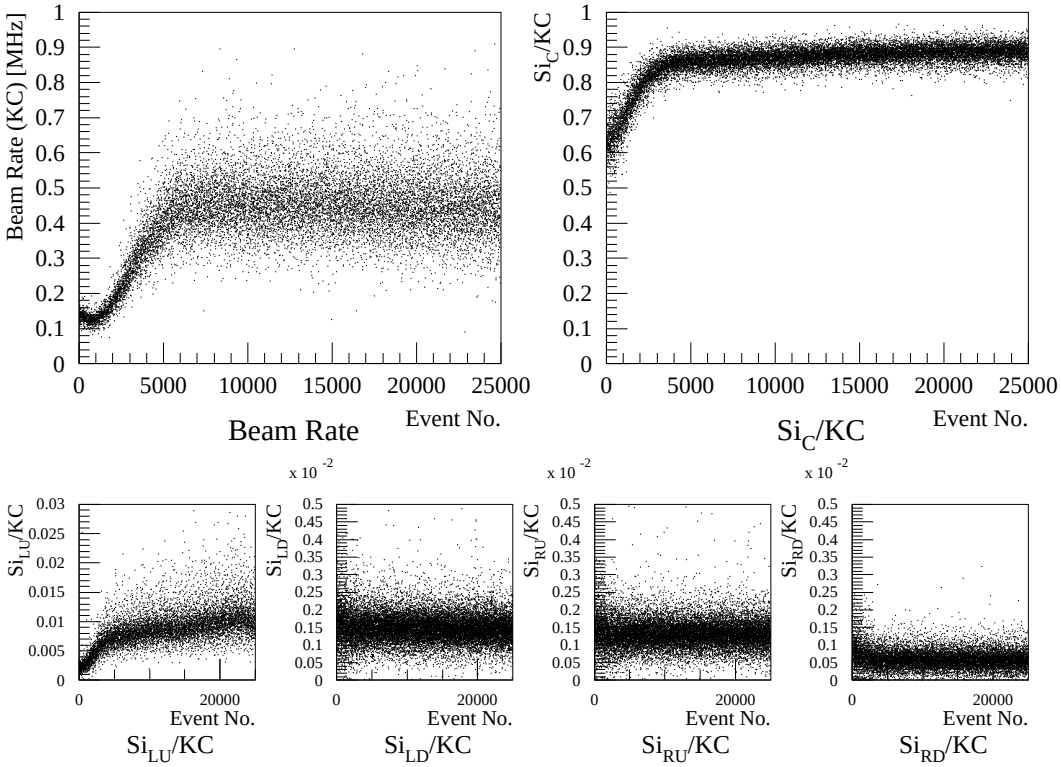


Figure 5: (from left to right) Beam Rate (Kens Chamber), Ratio of $Si_C/KC$, and $Si_{1-4}$ rate vs the event no. on tape (data for the finescan point at 1412 MeV/c).

# 3 Calculation of Cross Section

Now that it is shown that the scalers have reasonable values the next step is to calculate the cross sections. This will be done for the reactions $\bar{p}p \to \pi^0\pi^0$ and for a cross check with $\bar{p}p \to \pi^+\pi^-$. The normalization procedure will be shown in detail for the finescan data. A comparison will be made with the cross sections obtained for the same reactions at different momenta and the results will be discussed in detail. This will include also a discussion of the rate-dependence problem of David Bugg.

| $\bar{p}$ momentum [MeV/c] | $\sqrt{s}$ [MeV] | number of events |
|---|---|---|
| 1412 | 2223 | $7.30 \cdot 10^5$ |
| 1416 | 2224 | $4.74 \cdot 10^5$ |
| 1422 | 2226 | $5.67 \cdot 10^5$ |
| 1429 | 2229 | $8.31 \cdot 10^5$ |
| 1436 | 2231 | $9.65 \cdot 10^5$ |
| 1443 | 2234 | $4.65 \cdot 10^5$ |
| 1449 | 2236 | $4.55 \cdot 10^5$ |
| 1454 | 2237 | $4.13 \cdot 10^5$ |
| 1460 | 2239 | $6.60 \cdot 10^5$ |

Table 2: Momenta of incoming beam and statistics of the 9 finescan points

## 3.1 The Finescan Data

The Finescan was the subject of several talks by Kamal Seth, Jan Kisiel and myself at collaboration meetings, so details of the scan itself will not be given here (CB-note in preparation). To summarize the finescan in short: data was taken at 9 different momenta in the range of 1412 MeV/c to 1460 MeV/c in a total of two weeks of running. Table 2 summarizes the 9 scan points and the statistics of these points.

The scalers were read out as described in the first part of this note on an event to event basis, i.e. the difference of the scaler values of the actual event to the previous event was taken and this was then summed up over complete runs. In this way the error of taking the average of the scalers while beam conditions change should be minimized. In this same manner also the lifetime correction on the number of incoming antiprotons was done for every event and then summed up to get the total number of incoming antiprotons for whole runs, i.e. the number of antiprotons of a specific run arriving while

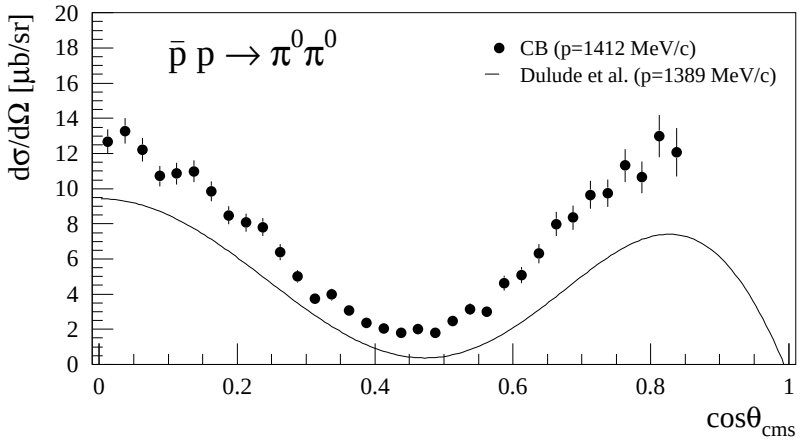


Figure 6: Angular Distribution of $\bar{p}p \to \pi^0\pi^0$ for the scan point at 1412 MeV/c incoming beam momentum. Solid line is the distribution for the measurement of Dulude et al. [3] at 1389 MeV/c

the trigger gate is open $N_{\bar{p}}$ is given by

$$N_{\bar{p}} = \sum_{\text{all events}} L \cdot KC.Si_C \quad ; \qquad L = \frac{t_{16\,MHz}}{t_{10\,kHz}}.$$

As mentioned above, $N_{barp}$ is determined event by event. Taking instead the total average of the lifetime $< L >$ multiplied by $\sum KC.Si_C$, as proposed [6], leads to errors in case of data samples with changing rates.

Using this number the differential cross sections for the reaction $\bar{p}p \to \pi^0\pi^0$ are calculated. With $N_{\pi^0\pi^0}$ the number of acceptance corrected $\pi^0\pi^0$ events and $R_{target}$ the 'reaction rate' in the target

$$R_{target} = \frac{1}{\rho_{H_2} \cdot \ell_{target} \cdot N_{Avogadro}} = 5.33 \cdot 10^6 \mu b \quad ,$$

the formula for the differential cross section then reads

$$\frac{d\sigma}{d\Omega} = \frac{N_{\pi^0\pi^0}}{N_{\bar{p}}} \cdot R_{target} \quad .$$

Figure 6 shows as a result of the normalization the angular distribution of $\bar{p}p \to \pi^0\pi^0$ up to $\cos(\theta) = .85$ for the first scan point with a momentum of the incident $\bar{p}$ of 1412 MeV/c. For comparison the same plot also shows the only other measurement of this reaction, but at a slightly different energy, made by Dulude et al. [3] It can be seen that whereas the shapes of the

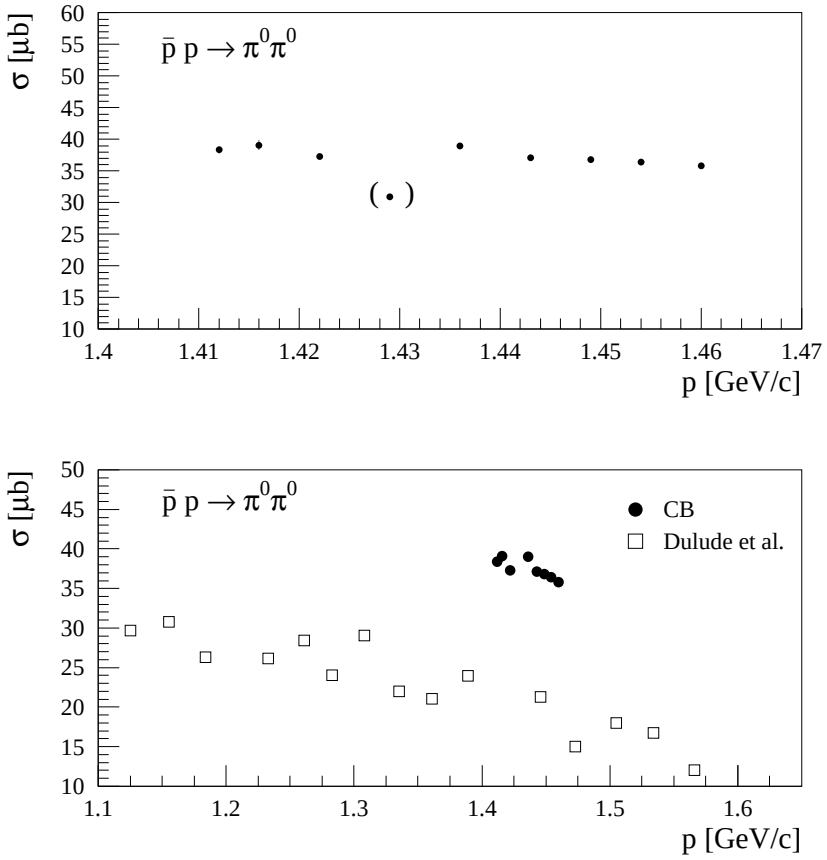


Figure 7: Excitation Function of $\bar{p}p \to \pi^0\pi^0$; the lower plot shows the cross section values in comparison to the cross section values as measured by Dulude et al. All values are the integrals of the angular distributions up to $\cos(\theta) < 0.85$

angular distribution are similar the overall values differ by up to a factor of 2. The discrepancy between the values of Dulude et al. and Crystal Barrel appears also clearly in the numbers of the integrated differential cross sections. Figure 7 presents the cross sections as a function of the incoming $\bar{p}$ momentum as measured by Crystal Barrel and Dulude et al. The cross section values for both measurements were evaluated by integrating the angular distributions in the range of $0 < \cos(\theta) < .85$

$$\sigma = 2\pi \int \frac{\mathrm{d}\sigma}{\mathrm{d}\Omega} \mathrm{d}(\cos\theta)$$

so the numbers can be compared directly. (The fact that there are identical particles in the final state was taken into consideration, i.e. only the forward

directed $\pi^0$ with a $\cos(\theta) > 0$ was used for the differential cross section, so every event is only counted once). It should be noted here that there is the scan point at 1429 MeV/c where the cross section appears to be significantly lower as for the other 8 scan points and is put into brackets in this presentation of the excitation function (in the lower plot this point was not included). For this special point problems were reported during data taking and the quality checks on the data showed peculiarities for the beam condition as was shown by Jan Kisiel at collaboration meetings (e.g. January 97). Thus the normalization to the number of incoming $\bar{p}$ was not used for the excitation function in this case but rather the normalization to the reaction $\bar{p}p \to \pi^0\pi^0\pi^0$.

Otherwise it appears that the remaining Crystal Barrel cross sections are almost constant for all scan points in the incoming momentum range but lie about 80% above the values of Dulude et al. This raises the question of the reliability of the Crystal Barrel normalization.

One way to gain some confidence in the measured Crystal Barrel values is by looking into reactions with charged particles in the final states. The reaction that suites our purposes best is $\bar{p}p \to \pi^+\pi^-$. It may be added that reactions $\bar{p}p \to$ *anything* and $\bar{p}p \to \bar{p}p$ were also taken into consideration. For the total $\bar{p}p$ cross section the idea was to count all events taken with the minimum bias trigger and to normalize this to the number of incoming $\bar{p}$. Although the resulting value of 82 mb turns out to fit quite well to the literature value of 97.7 mb there appear to be large uncertainties due to

- vetoing on reaction products
- inclusion of $\bar{p}p \to n\bar{n}$ in the data
- insufficient veto causing 'empty events'
- blind angle of about 12° in the forward direction causing a significant loss of events of the type $\bar{p}p$ *elastic* (approx. 10 mb).

This leads to an estimated relative error of about 30% that has to be assigned to the cross section value.

For the reaction $\bar{p}p \to \bar{p}p$ the problem arises that the opening angle in the lab-system is too small to make any useful analysis, even for a momentum of the incoming beam of 900 MeV/c.

So in the end the only useful reaction is $\bar{p}p \to \pi^+\pi^-$ despite a somewhat low total cross section of only about 150 $\mu$b. The selection of this channel required exactly 1 pos. charged long track (i.e. more than 9 hits in the JDC) and 1 neg. charged long track. Beside that any number of short tracks were

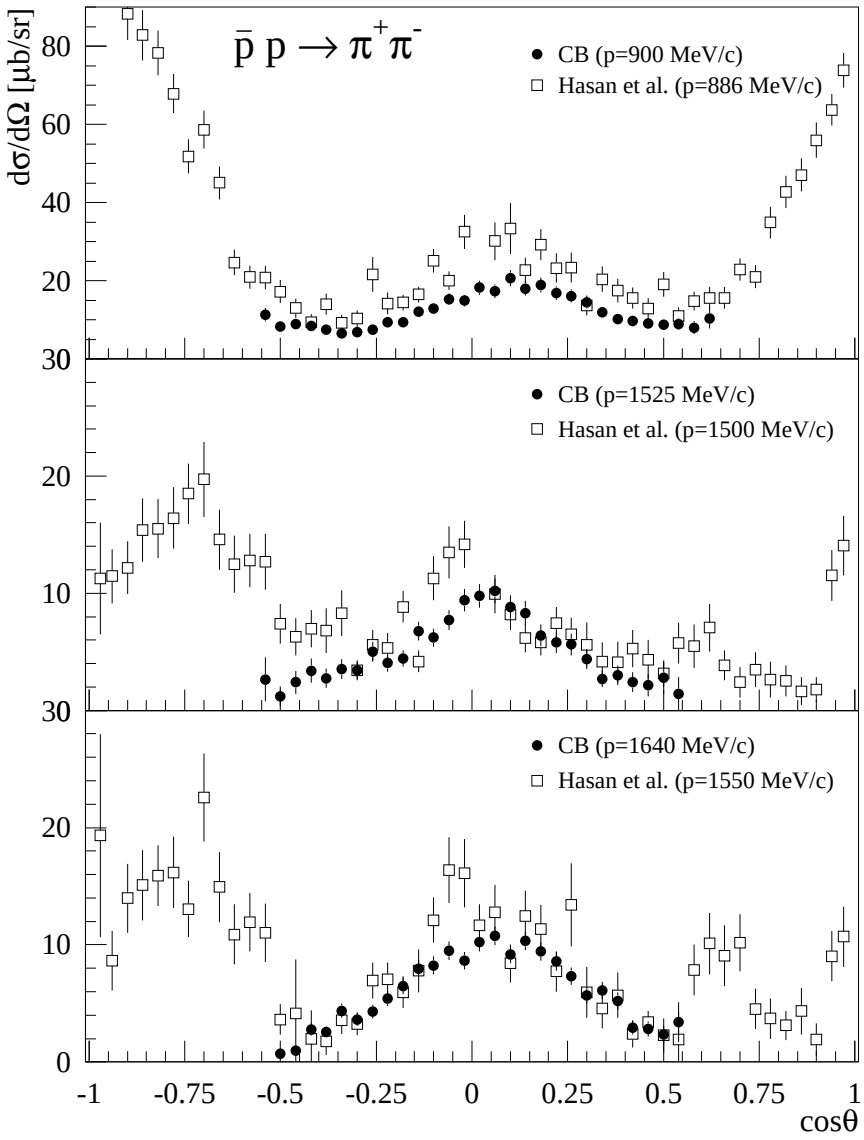


Figure 8: Angular distributions of $\bar{p}p \rightarrow \pi^+\pi^-$ for 3 different momenta of the incoming beam. Filled circles are the Crystal Barrel values, open boxes are the measurement of Hasan et al. [4]

allowed but not used in the analysis. (It turns out that after the final selection the number of events having a total of more than 2 tracks are less than 2% of all events). Also the crystal information was completely discarded. This avoids problems with hadronic split-offs. The two selected tracks were then passed on to the kinematic fit. The background on this selection was found to origin mainly from $\bar{p}p \to K^+K^-$ and to contribute less than 10%, increasing with the value of the incident momentum.

Figure 8 presents the angular distributions for $\bar{p}p \to \pi^+\pi^-$ for incident momenta of the antiproton of 900 MeV/c, 1525 MeV/c and 1642 MeV/c together with the measured values of Hasan et al. [4] at comparable momenta. The agreement of these two experiments looks quite encouraging but it should be pointed out that the agreement to the measurement of Eisenhandler et al. [5], which gives higher values for the $\pi^+\pi^-$ cross sections, is somewhat worse. Taking this into consideration it can be stated as a conclusion that the Crystal Barrel cross sections show a 'reasonable' consistency with previous measurements with the special remark that the CB cross sections lie systematically below the values of the other $\pi^+\pi^-$ experiments and by no means 80% above (as in the case of $\pi^0\pi^0$).

It remains to be shown that the results of the normalization, i.e. the cross sections are independent of the triggers used. For this reason the reaction $\bar{p}p \to \pi^0\pi^0$ was analyzed for data taken at the same momentum of 1525 MeV/c with the minimum bias trigger and with the 0-prong trigger. The same was done for $\bar{p}p \to \pi^+\pi^-$ comparing the minimum bias data with the 2-prong data. The results of this comparison are shown in Figure 9. For both reactions the angular distributions of the minimum bias triggered data with the 0-prong/2-prong data compare remarkably well. The difference in the integrated cross section up to $\cos(\theta) = 0.7$ is about 9% for the $\pi^0\pi^0$ final state and less then 4% for the $\pi^+\pi^-$ final state (cross section integrated in the range $|\cos(\theta)| < .5$ ). It should be noted here that the corresponding lifetime ratios of the data acquisition are factor 2.5 larger for the 2-prong trigger and factor 25 larger for the 0-prong trigger compared to the minimum bias lifetimes.

Summarizing it can be stated that the Crystal Barrel cross sections of the reaction $\bar{p}p \to \pi^0\pi^0$ lie about 80% above the values of the measurement of Dulude et al. Though cross checks with other channels are not exactly at the same energies a reasonable agreement of $\bar{p}p \to \pi^+\pi^-$ with previous measurements is found. A comparison of different triggers shows no dependence of the cross section results on the type of trigger. This indicates on the one hand that the lifetime measurement of the DAQ was done correctly. On the other hand it allows a direct comparison of the $\pi^+\pi^-$ cross sections

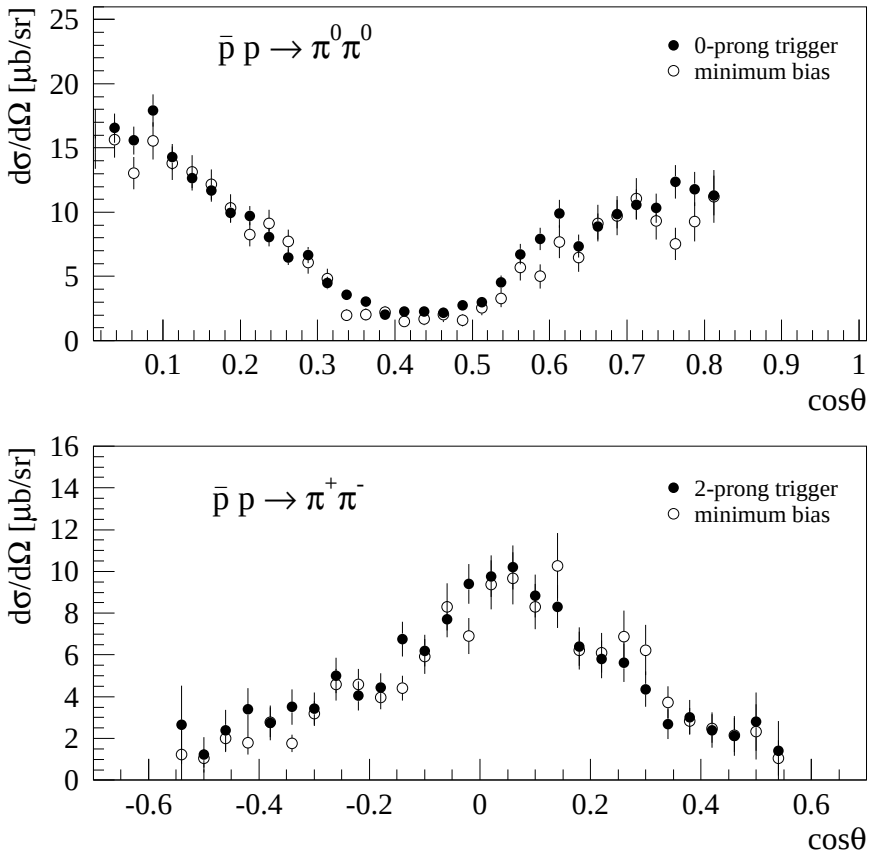


Figure 9: Comparison of the results using different triggers at the same $\bar{p}$ momentum of 1525 MeV/c. Upper plot shows the angular distribution of $\bar{p}p \to \pi^0\pi^0$ for data taken with the 0-Prong trigger (filled circles) and for minimum bias data (open circles). Lower plot shows the same for $\bar{p}p \to \pi^+\pi^-$ from the data of the 2-Prong trigger (filled circles) and for minimum bias data (open circles)

with $\pi^0\pi^0$ which excludes cross section values for $\bar{p}p \to \pi^0\pi^0$ in the range of Dulude et al. Taking this into account we believe the Crystal Barrel cross sections give the right results.

## 3.2 Discussion of Beam Rate Dependence

This section will give a discussion of what is known as 'beam rate' dependence for the finescan runs. David Bugg claimed this rate dependence in his Cb-note 335 on the 'Normalization of in-flight data' [6] and recently for the finescan in the addendum to this note (CB-note 336) [7].

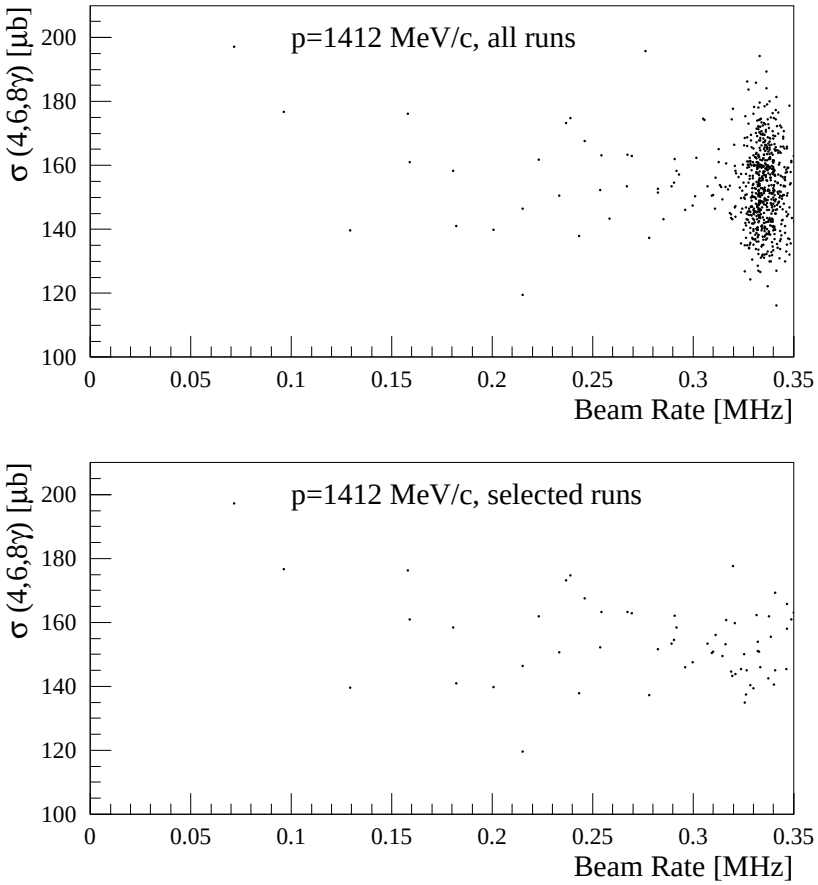


Figure 10: Cross section of $4\gamma$, $6\gamma$ $8\gamma$ events vs. beam rate for the incoming beam momentum of 1412 MeV/c. Upper plot shows all runs, lower plot only the runs selected by David Bugg [7] (runs 42053, 42058 and 42060).

To try to compare the results of this analysis with the results of David Bugg just about the same procedure was used in the analysis. Every run was split up into successive groups of 1000 events. These events run through the analysis, selecting final states with $4\gamma, 6\gamma$ and $8\gamma$ and kinematically fitting

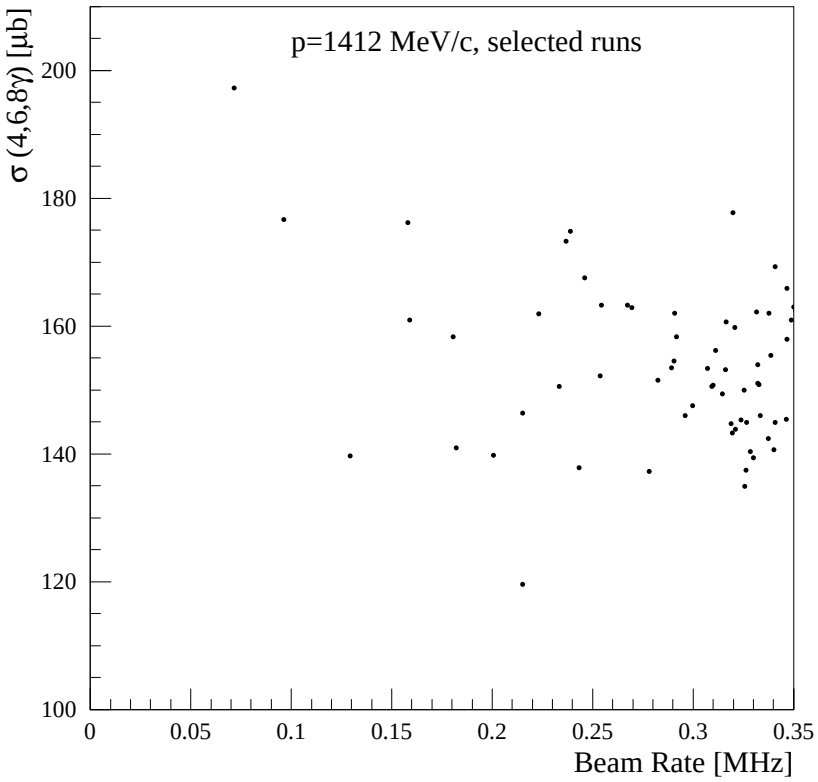


Figure 11: Cross section of $4\gamma, 6\gamma$and$8\gamma$ events vs. beam rate for the incoming beam momentum of 1412 MeV/c for selected runs [7] (same as previous plot, only different scale to compare with David's presentation).

them then to these final states. Events with confidence level larger 1% were accepted. It should be mentioned that the present data samples and those of [6] [7] are not exactly the same. In contrary to [6] [7] the events once passing the 4, 6 or 8 $\gamma$ hypothesis are not additionally fitted to specific final states, also 5 and 7$\gamma$ events are not selected but correlations between the normalization and the beam rate do not depend significantly on the numbers of $\gamma$s.

Figure 10 shows the cross section vs. the average beam rate as measured for each group of 1000 events for the first scan point at an incoming momentum of 1412 MeV/c. It should be added that the 'cross sections' noted in the following for the 4$\gamma$, 6$\gamma$ and 8$\gamma$ final states are not acceptance corrected (in contrary to the $\pi^0\pi^0$ and $\pi^+\pi^-$ final states above), which is not important in the present context. The upper plot shows the results for all runs of this scan point, the lower plot for the runs 42053, 42058 and 42060 as presented by David Bugg [7]. For these selected runs there seems to be an indication of a weak beam rate dependence. To enhance this effect the same runs were plotted in a different presentation in Figure 11. But if all the runs are taken into account and the spread of the points at the great bulk at a beam intensity of about 0.34 MHz is taken into consideration the rate dependence gets less obvious if not disappears at all in the range of the distribution.

Figures 12, 13 and 14 show the same for the scan point at 1416 MeV/c, 1422 MeV/c and 1436 MeV/c momentum of the incoming beam. For 1416 MeV/c the selected runs are 42088, 42092 and 42109 [7]. A comparison of the presentation using all the runs again indicates the same as for the runs at 1412 MeV/c. At 1422 MeV/c the runs are divided into two groups [7], first group covering run numbers below 42124 and the second group with runs above run number 42125. These runs seem to show a beam rate dependence for low beam rates. On the other hand both groups as well as all runs display two areas where the bulk of the data lie, one at a beam rate of 0.19 MHz and one at a slightly higher beam rate but well separated from the other at 0.24 MHz. Both areas are centered at the same cross section value of 150 MeV/c and are in disagreement with any straight line drawn through the points with lower beam rates.

For runs 1436 MeV/c the selected runs are 42412, 42424, 42441, 42449 and 42459 [7]. A rate dependence in the selected runs is hard to see.

Close inspection of Figures 12, 13 and 14 reveals a large number of points in the low-rate region of the upper plots that do not enter into the selection [7] presented in the lower plots (in addition to the greater bulk).

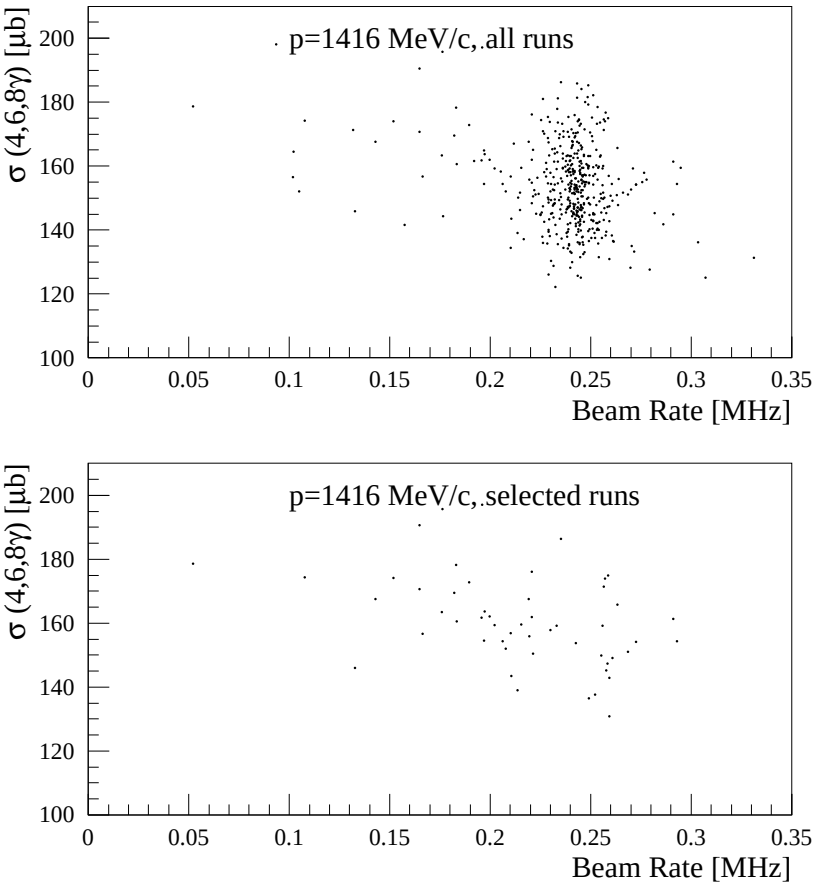


Figure 12: Cross section of $4\gamma$, $6\gamma$ and $8\gamma$ events vs. beam rate for the incoming beam momentum of 1416 MeV/c. Upper plot shows all runs, lower plot only for selected runs [7] (runs 42088, 42092 and 42109).

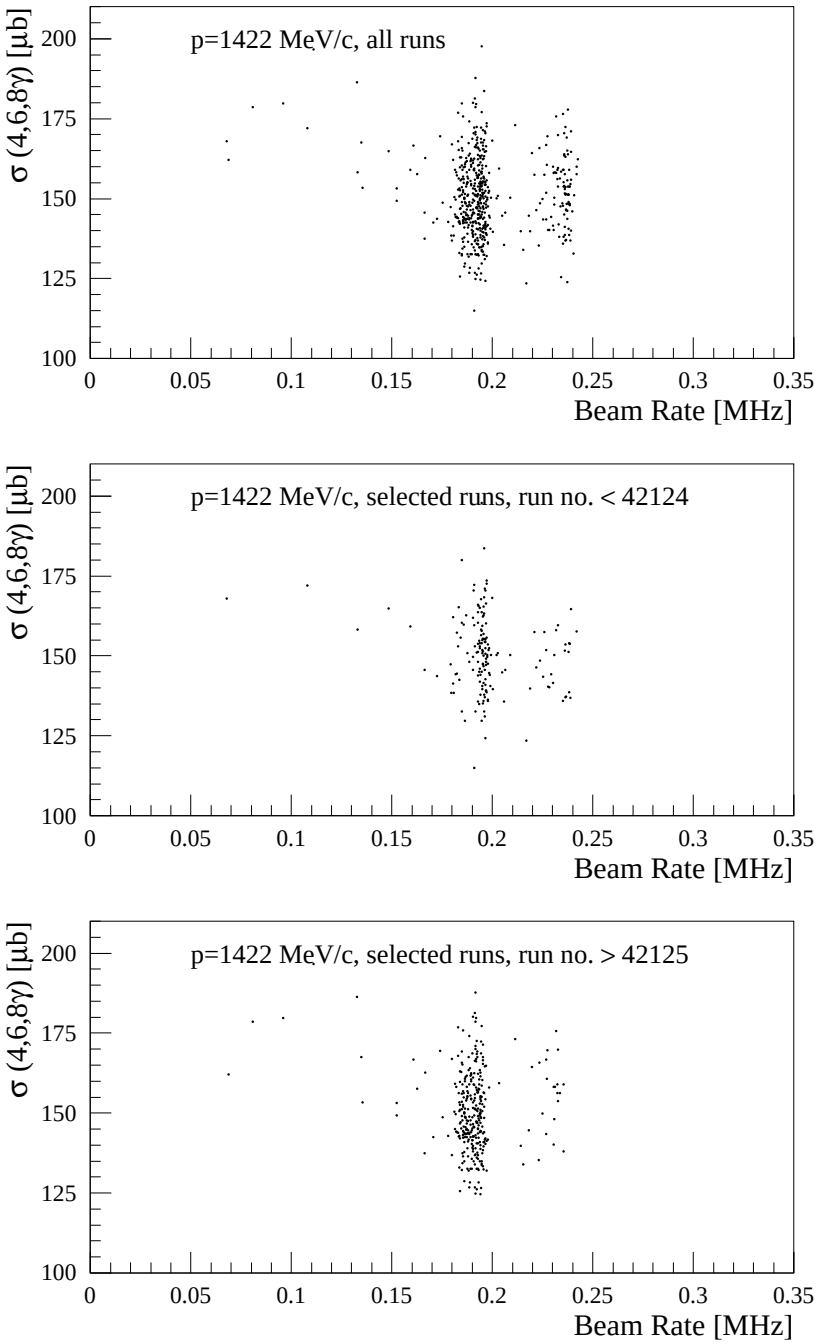


Figure 13: Cross section of $4\gamma$, $6\gamma$ and $8\gamma$ events vs. beam rate for the incoming beam momentum of 1422 MeV/c. Upper plot shows all runs. The plot in the middle shows runs with run no. below 42124 the plot on the bottom the runs with run no. above 42125 [7].

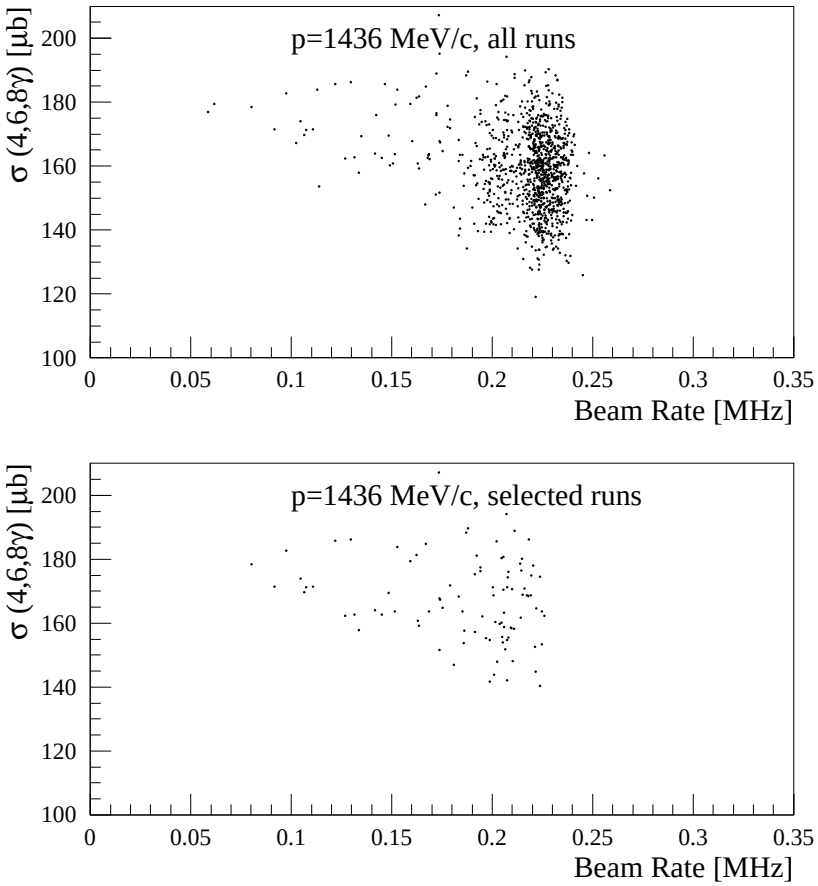


Figure 14: Cross section of $4\gamma$, $6\gamma$ and $8\gamma$ events vs. beam rate for the incoming beam momentum of 1436 MeV/c. Upper plot shows all runs, lower plot only selected runs [7] (runs 42412, 42424, 42441, 42449 and 42459).

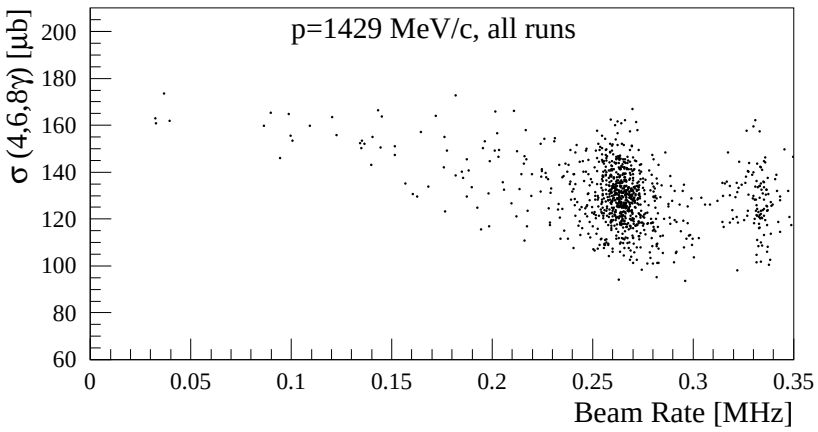


Figure 15: Cross section of $4\gamma$, $6\gamma$ and $8\gamma$ events vs. beam rate for the incoming beam momentum of 1429 MeV/c - the momentum where normalization to the incoming $\bar{p}$ was not used in the excitation function due to the abnormal beam conditions. Clear 'rate dependence' can be seen.

For the runs at 1429 MeV/c the situation concerning beam rate dependence seems a bit clearer as for the other scan points. The exceptional bad beam quality at this energy was already mentioned before and was the reason to avoid the normalization to the incoming $\bar{p}$ of this scan point for the excitation function. Figure 15 presents the 4, 6 and $8\gamma$ cross sections vs. the beam rate of the groups of 1000 events for all runs of this scan point. There are two main groups of points at beam rates of 0.26 MHz and 0.33 MHz both lying about 15% below the average of the other values. Here the distributions as a whole increase with the beam momentum and a simple approximation with the weight on the points of lower beam rate leads to a cross section value of 180 $\mu$b at 0 beam intensity. If one however draws a line through the 2 points where the bulk of the data sits the extrapolation to beam rate 0 gives approx. 150 $\mu$b - the value of the average of the other scan points. It is not the intention of this note to suggest this or that kind of extrapolation but to make aware of the different kinds of interpretation the cross section allow in this case. To stand on firm ground anyhow for the analysis of the finescan any interpretation of the cross section of this point is avoided and rather a normalization to the $\bar{p}p \to \pi^0\pi^0\pi^0$ reaction was chosen.

Figure 16 presents the first three scan points vs. beam rate in one plot. First of all it can be seen that the runs at these three points show rather different beam rates with a rate of 0.34 MHz for the runs at 1412 MeV/c,

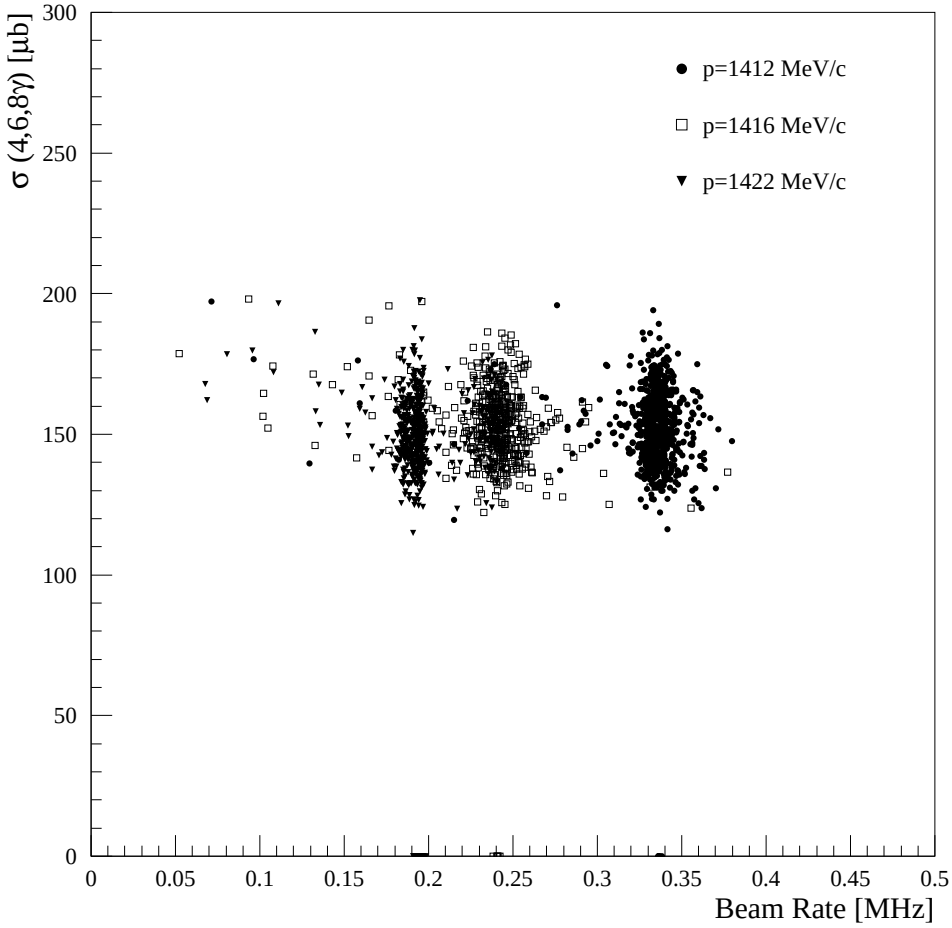


Figure 16: Cross sections for 4, 6 and 8 $\gamma$ events vs. beam rate for momenta of incoming beam of 1412 MeV/c, 1416 MeV/c and 1422 MeV/c.

0.24 MHz at 1416 MeV/c and 0.20 MHz at 1422 MeV/c. The big bulk of points are all centered at the same value of cross section at about 150 $\mu$b. It should also be noted that at places where the points of different scan points have the same beam rate the distributions overlap as to be seen at 0.24 MHz beam rate where some runs of the scan point of 1422 overlap with the point of 1416 MeV/c. This leads immediately to a difficulty of the beam rate interpretation. If the points where the beam rate is kept constant have the same cross section values for different beam intensities and an extrapolation for these points to beam rate 0 should lead to just about the same values for cross section again then the slopes for the straight lines giving these extrapolations have to be significantly different. This raises doubt whether the effect indicated in the selected runs is really a simple beam rate dependence since then the same slope for all points would be required. The only way to explain different slopes would be to include more parameters probably some kind of beam condition.

A linear fit to all points in Figures 10, 12, 13 and 14 (upper plots) yields the following values for the 'cross section' $\sigma(0)$ at rate 0, in comparison with fitting a constant, rate independent $\sigma_{\mathrm{const}}$:

| momentum [MeV/c] | $\sigma(0)$ [$\mu$b] | $N_{dof}$ | $\chi^2/N_{dof}$ | $\sigma_{\mathrm{const}}$ [$\mu$b] | $\chi^2/N_{dof}$ |
|---|---|---|---|---|---|
| 1412 | $170.1 \pm 6.0$ | 710 | 1.10 | $151.8 \pm 0.4$ | 1.11 |
| 1416 | $184.5 \pm 5.0$ | 463 | 1.03 | $152.7 \pm 0.6$ | 1.12 |
| 1422 | $159.6 \pm 4.7$ | 532 | 1.01 | $149.9 \pm 0.6$ | 1.01 |
| 1436 | $185.7 \pm 3.8$ | 1089 | 1.01 | $157.9 \pm 0.4$ | 1.06 |

Hence, if one follows the concept of a rate dependent cross section, the $\sigma_{\mathrm{const}}$ value is 17% too low in the worst case (1416 MeV/c) and correct within statistics in the best case (1422 MeV/c). This is in contrast to the large effects claimed for the selected runs at the same momenta in [7].

### 3.3 Beam Rate Dependence due to Pile-Up Effects?

Pile-up would occur when an event is accepted but a calorimeter crystal still shows some afterglow from the previous (rejected) event. Thus the number of PEDs of the accepted event would increase and with that also the total energy and momentum. This would finally lead to the rejection of good events during the analysis. Such a pile-up effect would indeed give a simple explanation for a beam rate dependence, the higher the beam intensity the higher the pile-up rate.

To investigate the effect of pile-ups the same groups of 1000 events were used as above and the number of $4\gamma$, $6\gamma$ and $8\gamma$ events out of these groups

were counted and plotted against the beam rate. With no (rate dependent) pile-up one would expect that the number of $4\gamma$, $6\gamma$ and $8\gamma$ events would then be constant. A pile-up effect depending on the beam intensity however would mean that the absolute number of selected events from these 1000 events should increase with decreasing beam intensity, simply because the number of pile-up should be reduced. The lower plot of Figure 17 shows the number of 4, 6 and $8\gamma$ events vs. the beam rate together with the $1\sigma$ error of the number of events . The upper plot displays the way this error was estimated. The number of 4, 6 and $8\gamma$ events were simply filled in a histogram and fitted to a gaussian. The standard deviation $\sigma$ is found to be consistent with the value expected from Poisson statistics $\sqrt{\mathrm{N} \cdot \mathrm{P}(\overline{4\gamma, 6\gamma, 8\gamma})}$ , where the probability $\mathrm{P}(\overline{4\gamma, 6\gamma, 8\gamma})$ for an event to be not of the $4\gamma, 6\gamma, 8\gamma$ type is about 83%. The distribution of selected events vs. beam rate show no evidence of a beam rate dependence. All points including those at low beam rate are nicely distributed around the 1 $\sigma$ area. Figure 18 shows the corresponding distribution for the scan points at 1416 MeV/c, 1422 MeV/c and 1436 MeV/c incoming beam momentum. Though there is some indication of an increase of the number of events with decreasing beam intensity, its statistical significance is rather poor.

For the runs at 1429 MeV/c however the situation turns out very clear as can be seen in Figure 19. Here systematically all points at lower beam intensity lie outside of the 1 $\sigma$ area which could be an indication for a pile-up effect.

The data plotted in Figures 17 - 19 differ from those of the previous section (Figures 10 - 16) only by the normalization factor, i.e. the number $\mathrm{N}_{\bar{\mathrm{p}}}$ of $\bar{\mathrm{p}}$'s per 1000 events and the overall normalization factor, i.e. $5.33 \cdot 10^6$ mb/$\mathrm{N}_{\bar{\mathrm{p}}}$. Consistency of the above considerations demands that this normalization factor should not depend signicantly on the beam rate. This is shown in Figure 20. It confirms that the beam rate dependence at 1429 MeV/c (Fig. 15) comes essentially from the different number of events passing the selection of the final state.

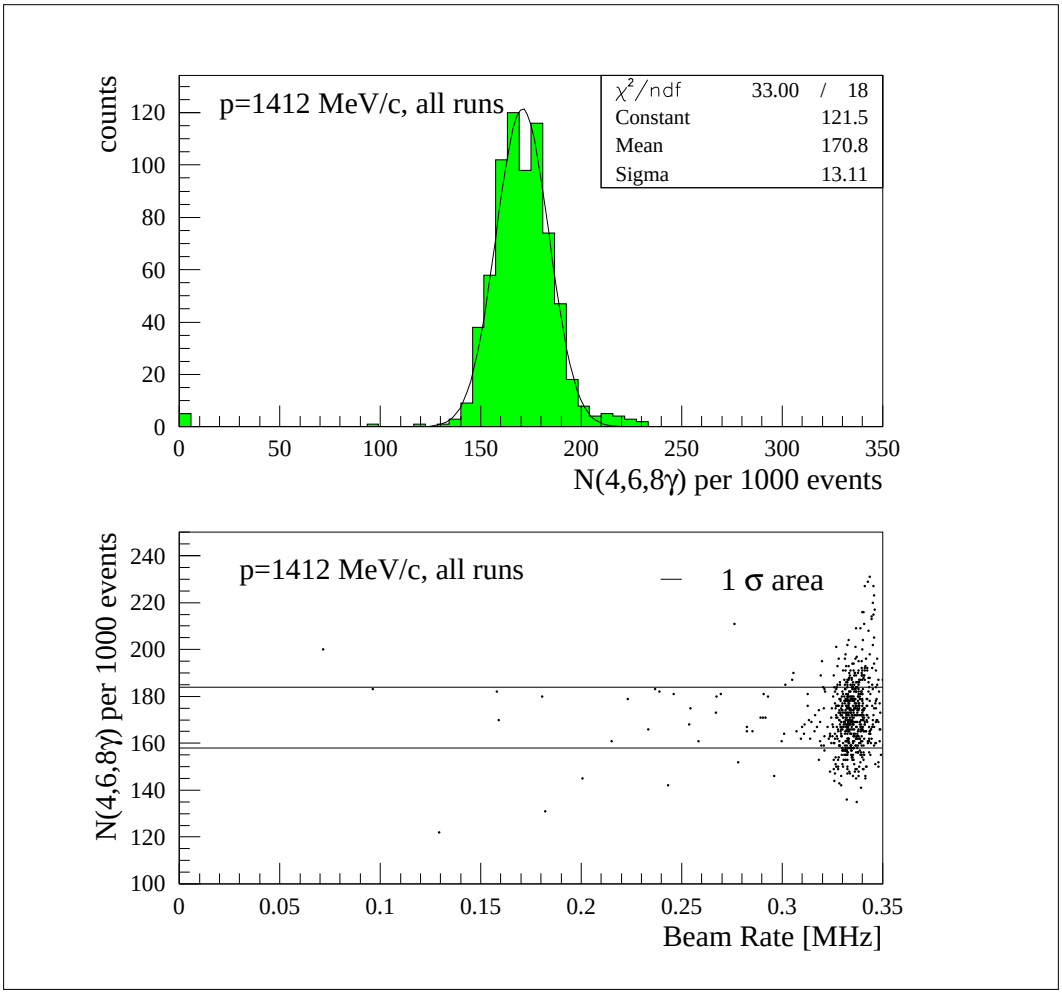


Figure 17: Number of $4\gamma + 6\gamma + 8\gamma$ events per 1000 events on tape for incoming momentum of 1412 MeV/c. Upper plot shows the result of a gaussian fit to the distribution, lower plot shows the number of $4\gamma + 6\gamma + 8\gamma$ events vs. the beam rate with the $1\sigma$ boundary. No 'rate dependence' visible.

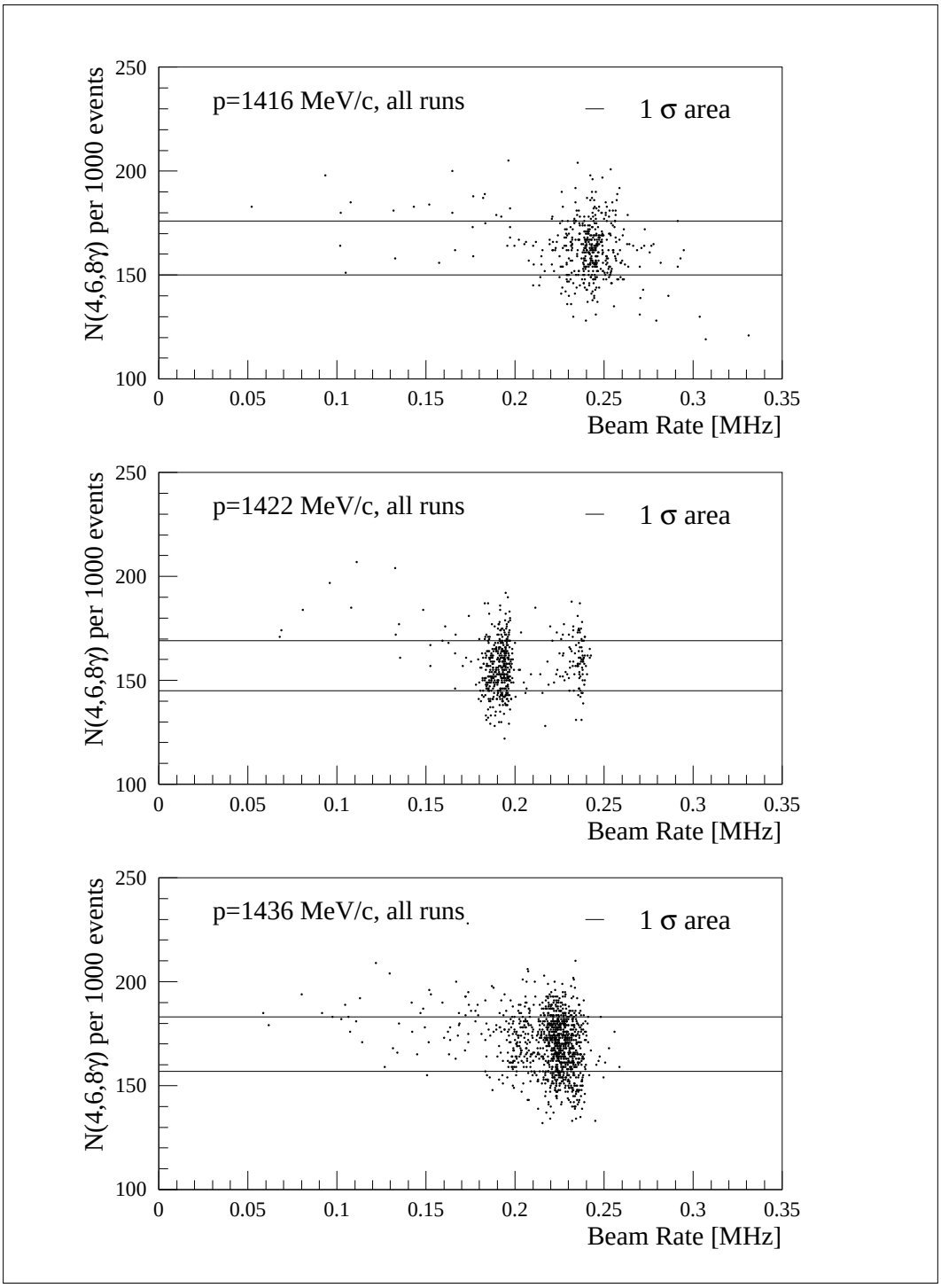


Figure 18: Number of $4\gamma + 6\gamma + 8\gamma$ events per 1000 events vs. beam rate for incoming momenta of 1416 MeV/c, 1422 MeV/c and 1436 MeV/c. The solid lines show the $1\sigma$ area.

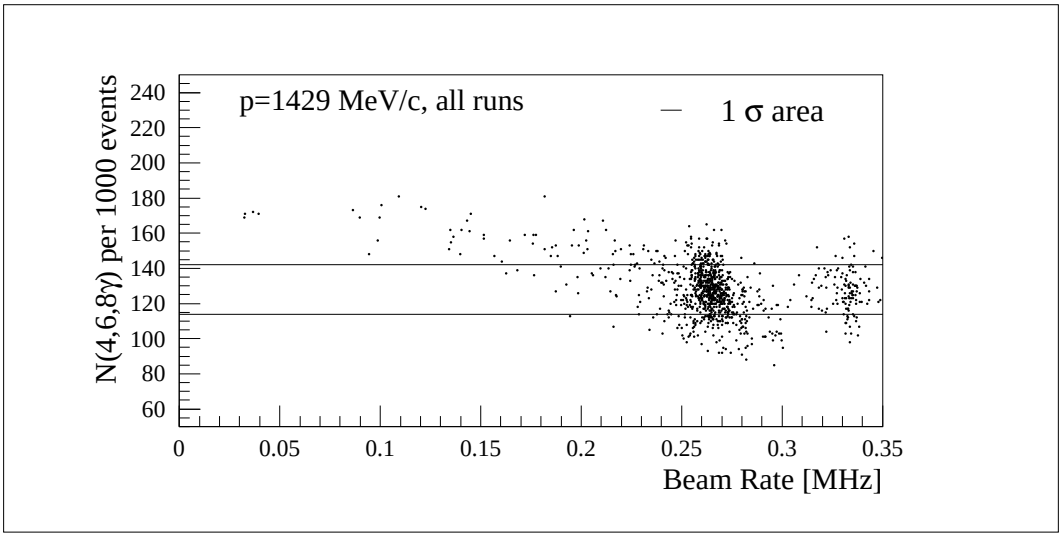


Figure 19: Number of $4\gamma + 6\gamma + 8\gamma$ events per 1000 events vs. beam rate for incoming momenta of 1429 MeV/c, solid line again showing the $1\sigma$ boundary.

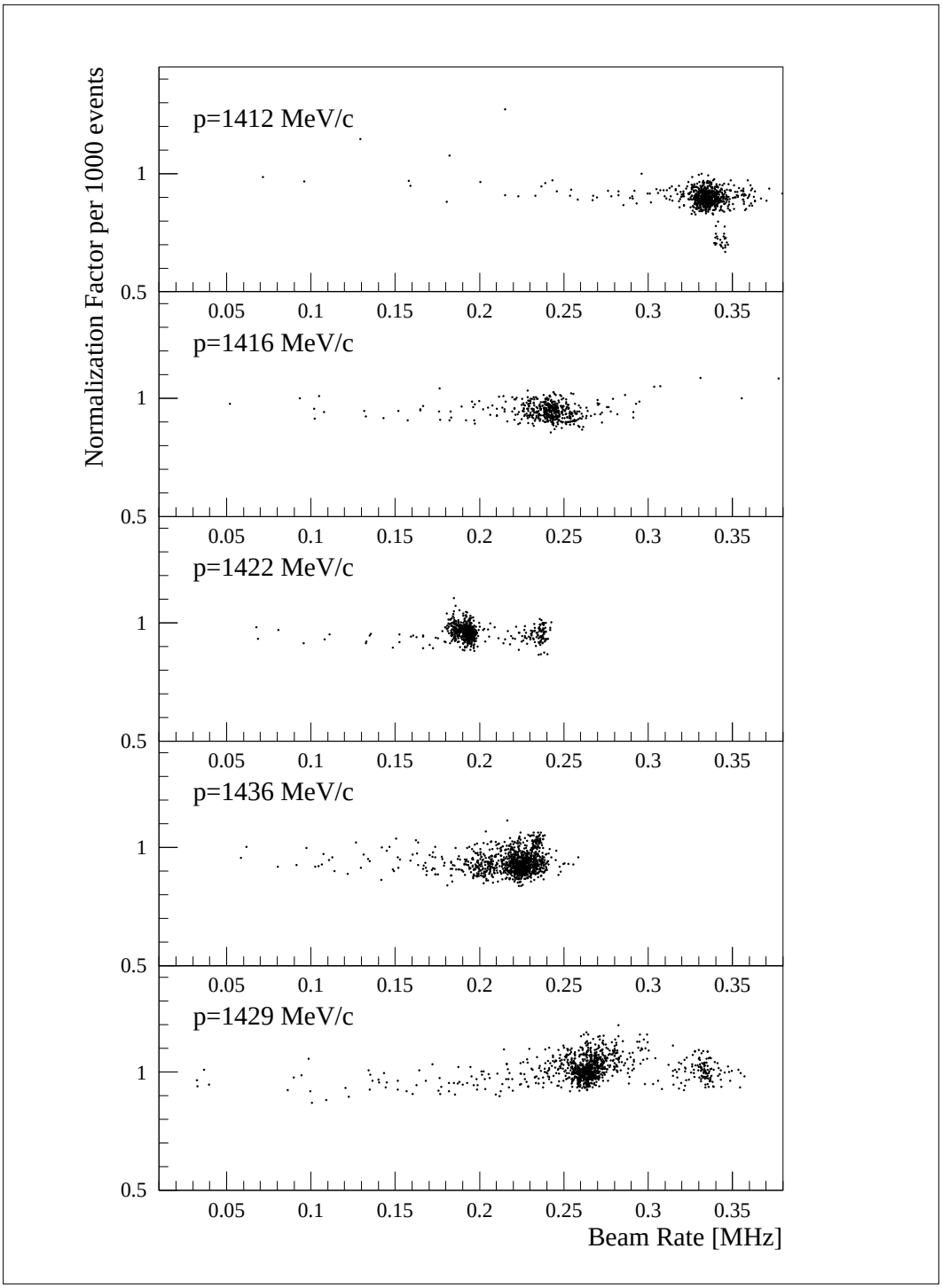


Figure 20: Normalization factor ($= 5.33 \cdot 10^6/N_{\bar{p}}$) of groups of 1000 events vs. beam rate for various incoming momenta. No rate dependence can be seen.

# Conclusion

- The cross section values for the reaction $\bar{p}p \to \pi^0\pi^0$ integrated over the range of $0 < \cos(\theta) < .85$ using the normalization methods described in this report are:

| $\bar{p}$ momentum [MeV/c] | cross section [$\mu$b] |
|---|---|
| 1412 | $38.4 \pm 0.6$ |
| 1416 | $39.1 \pm 0.7$ |
| 1422 | $37.3 \pm 0.6$ |
| 1436 | $39.0 \pm 0.5$ |
| 1443 | $37.1 \pm 0.6$ |
| 1449 | $36.8 \pm 0.6$ |
| 1454 | $36.4 \pm 0.6$ |
| 1460 | $35.8 \pm 0.5$ |

  - The estimated systematic error is 10% as judged by comparison of different triggers and 5% comparing different analysis methods (e.g. analysis of Jan Kisiel).
  - The relative error however between neighboring scan points of the finescan is close to the statistical one given in the table above. In fact they are spread around their average of 37.5 $\mu$b with a standard deviation of 1.1 $\mu$b.

- Checks of the normalization include the reaction $\bar{p}p \to \pi^+\pi^-$ and results for cross sections from data from different triggers. A reasonable agreement with previous measurements is found for the reaction $\bar{p}p \to \pi^+\pi^-$. The comparison of different trigger types shows a very good agreement of the results and confirms the independence of the results from the trigger used.

- One scan point at 1429 MeV/c, which is known to be problematic from the quality checks during data production, gives a cross section value about 20% less than the other scan points ($30.9 \pm 0.5$). In the forthcoming publication this point will be normalized to the yield of the reaction $\bar{p}p \to \pi^0\pi^0\pi^0$ which leads to a cross section in the region of the other points.

- No significant change of the normalization was found with the beam rate with the exception of the one scan point mentioned above. For a few selected runs at the other scan points a weak correlation of the normalization with the rate exists.

# Appendix A

The original scaler bank description by H. Kalinowsky.

```
================================================================================
                  SCALER BANK DESCRIPTION


VERSION OCT. 1993

CREATED :     2.JUL.90           H.KALINOWSKY
        UPDATED :    19.DEC.90           H.K
        UPDATED :    24.JUL.93           H.K
        UPDATED :    08.OCT.93           H.K
        UPDATED :    21.JUL.96           H.K

================================================================================

The scaler zebra bank contains the content of the Trigger scalers.
All scalers are 32 bit long, except the light and ameri scalers.
The first 20 scalers (scaler 1 to 16 are cascaded) are hard wired and have
the following meaning.
The data structure is the following:
               ------------------------------------
bankpointer+1  |     wordcounter of bank           | integer*4
               ------------------------------------

               ------------------------------------
bankpointer+2  |   scaler 1 lsb  |  scaler 1 msb   | integer*4
               ------------------------------------

               ------------------------------------
bankpointer+3  |   scaler 3 lsb  |  scaler 3 msb   | integer*4
               ------------------------------------

               ------------------------------------
bankpointer+4  |   scaler 5 lsb  |  scaler 5 msb   | integer*4
               ------------------------------------
                                 :
                                 :
               ------------------------------------
bankpointer+9  |   scaler 15 lsb |  scaler 15msb   | integer*4
               ------------------------------------

               ------------------------------------
bankpointer+10 |   scaler 18     |  scaler 17      | integer*4
               ------------------------------------

               ------------------------------------
```

```
bankpointer+11 |   scaler 20     |  scaler 19      | integer*4
               -------------------------------------

!!!!! MSByte and LSByte swapped from this location on

               -------------------------------------
bankpointer+12 |   scaler 21 msb |  scaler 21 lsb  | integer*4
               -------------------------------------
               -------------------------------------
bankpointer+13 |   scaler 23 msb |  scaler 23 lsb  | integer*4
               -------------------------------------
                                 :
                                 :
               -------------------------------------
bankpointer+27 |   scaler 51 msb |  scaler 51 lsb  | integer*4
               -------------------------------------



16 bit 16bit
Scaler 1 lsb msb sili r/down
Scaler 3  "  " sili l/down
Scaler 5  "  " sili r/up
Scaler 7  "  " sili l/up
Scaler 9  "  " sili center
Scaler 11  "  " Ken counter
Scaler 13  "  " or sili high tresh.
Scaler 15  "  " test pulser
Scaler 17  "   light 1
Scaler 18  "   ameri 1
Scaler 19  "   light 2
Scaler 20  "   ameri 2

The following 32 scalers are cascaded and are programable through
the trigger setup. The meaning of each counter is defined in the
triggerdescription file xxxx.dsc.


16bit 16bit
Scaler 21 msb lsb plu1/out6  (17)
Scaler 23  "  " plu2/out5  (18)
Scaler 25  "  " plu2/out6  (19)
Scaler 27  "  " plu3/out5  (20)
Scaler 29  "  " plu3/out6  (21)
Scaler 31  "  " plu4/out4  (22)
Scaler 33  "  " plu4/out5  (23)
```

```
Scaler 35  "  " plu5/out6  (24)
Scaler 37  "  " plu5/out7  (25)
Scaler 39  "  " plu6/out6  (26)
Scaler 41  "  " plu8/out6  (27)
Scaler 43  "  " plu7/out6  (28)
Scaler 45  "  " plu7/out7  (29)
Scaler 47  "  " event accepted  (30)
Scaler 49  "  " fast reset      (31)
Scaler 51  "  " system reset    (32)
```

Jul 96: There are 4 additional Scalers added for Lifetime measurements. Two counters are cascaded to form 32-Bit Scalers. The first is counting the Time between opening of the Triggergate and closing after a trigger was seen with a delay of 2400 nsec (Clockrate 16 MHz). The second has the identical gating, but 1 1MHz clock.

```
                 --------------------------------------
bankpointer+28   |   scaler 1 lsb  |  scaler 1 msb   | integer*4
                 --------------------------------------

                 --------------------------------------
bankpointer+29   |   scaler 3 lsb  |  scaler 3 msb   | integer*4
                 --------------------------------------
```

```
16 bit 16bit
Scaler 52 lsb msb Life Time 16 MHz
Scaler 54  "  " Life Time  1 MHz
```

# Appendix B

Listed below is the function SCL_FSWAP written by Klaus Peters and originally used in the trigger monitor program to extract values from the scaler bank.

```
*CMZ :          22/10/96  11.55.43  by  Unknown
*-- Author :    orig. K. Peters

      REAL FUNCTION SCL_FSWAP(I)
      IMPLICIT NONE

      INTEGER I, J, JBYT
      EXTERNAL JBYT

      SCL_FSWAP = FLOAT(JBYT(I,1,16))*65536. + FLOAT(JBYT(I,17,16))

      RETURN
      END
```

# References


[1] G. Folger, M. Doser, Ch. Voelcker, Offline Reconstruction Software Vers. 1.27/00, CB-Note 121 (1995)

[2] Klaus Peters, email to the collaboration, Aug 98;
Jamboree 97 minutes

[3] R.S. Dulude et al., Phys. Lett. B79 (1978) 329;
R.S. Dulude et al., Phys. Lett. B79 (1978) 335

[4] A. Hasan et al., Nucl. Phys. B378 (1992) 3

[5] E. Eisenhandler et al., Nucl. Phys. B96 (1975) 109

[6] D. Bugg and A.V. Sarantsev, Normalisation of in-flight data, CB-Note 335

[7] D. Bugg and A.V. Sarantsev, Addendum on In-Flight Normalisation, CB-Note 336